Free Surface Flow in the Mixing Zone of an Annular Centrifugal Contactor

Kent E. Wardle, Todd R. Allen, and Mark H. Anderson
Dept. of Engineering Physics, University of Wisconsin-Madison, Madison, WI 53706

Ross E. Swaney
Dept. of Chemical and Biological Engineering, University of Wisconsin-Madison, Madison, WI 53706

DOI 10.1002/aic.11381
Published online December 3, 2007 in Wiley InterScience (www.interscience.wiley.com).

The annular centrifugal contactor has been developed as the central piece of equipment for advanced liquid–liquid extraction processes for use in recycling spent nuclear fuel. While a sufficient base of experience exists to support successful operation of current contactor technology, a more complete understanding of the fluid flow within the contactor would enable further advancements in design and operation of future units. In particular, an important characteristic of the flow that is not well understood and which significantly complicates computational modeling of the contactor is the complex free surface flow in the annular mixing zone. This study presents the results of time-dependent, multiphase computational fluid dynamics (CFD) modeling using the volume-of-fluid (VOF) interface tracking method to characterize the mixing zone in a model centrifugal contactor. Laser doppler velocimetry (LDV) measurements of the actual flow velocities within the contactor were also performed. The experimental results were compared with simulations using various turbulence modeling schemes. The CFD model predictions using a coarse grid large eddy simulation (LES) method are in good agreement with the experimental measurements and observations. © 2007 American Institute of Chemical Engineers *AIChE J,* 54: 74–85, 2008

Keywords: computational fluid dynamics (CFD), nuclear engineering, multiphase flow, mixing, liquid–liquid extraction

Introduction

Among the many types of process equipment which are applicable to solvent extraction,[1–3] liquid–liquid extraction columns (originally packed and later pulsed columns) and mixer-settlers have traditionally been used for spent fuel reprocessing.[4] The annular centrifugal contactor has several important advantages over these other types of equipment.[5–7] Centrifugal contactors are compact and have a relatively short fluid residence time and small liquid volume hold-up resulting in reduced solvent exposure to radiation, and consequently, decreased solvent degradation. This can be particularly vital for processes which employ sensitive or expensive solvents and/or extractants.[8,9] Their small size also reduces physical space requirements, improves nuclear criticality safety, and enables quick startup and shutdown. Despite the short residence time and small size, contactors also have very high extraction efficiency and high throughput. Further, annular centrifugal contactors can operate over a wide range of organic to aqueous flow ratios (O/A) making them a versatile piece of equipment for a wide range of solvent extraction processes.

The initial design of the annular centrifugal contactor was made at Argonne National Laboratory by modification of a Savannah River Laboratory (SRL) contactor as described by

Correspondence concerning this article should be addressed to K. E. Wardle at kwardle@wisc.edu.

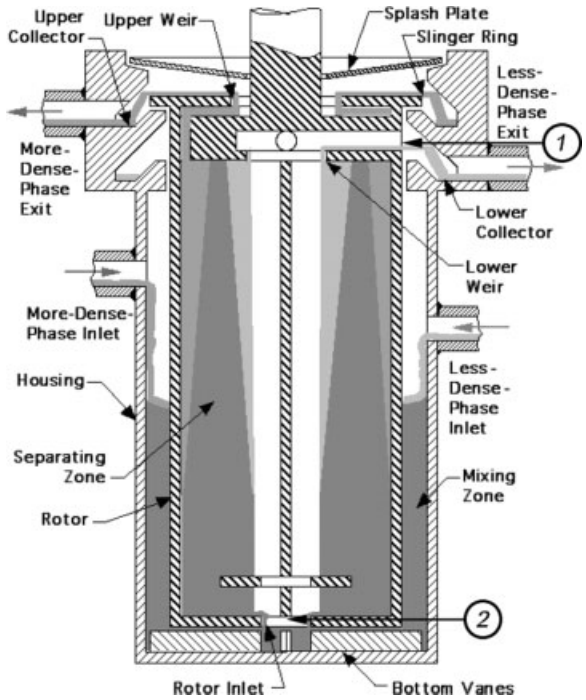

Figure 1. Sketch of the cross-section of an annular centrifugal contactor with the main components labeled.

Figure taken from Leonard et al. 2002.[14]

Bernstein et al.[10] Groups in Japan[7] and China[11] have also developed annular centrifugal contactors based on the Argonne design. Others have also developed similar equipment based on the same principles.[12,13] A cross-section for a general Argonne contactor is shown in Figure 1. Contactors are typically referred to by the diameter of the rotor. Hence, a 5-cm contactor is an annular centrifugal contactor with a 5-cm diameter rotor.

Centrifugal contactors will be critical to the success of the future advanced fuel reprocessing facilities which have been recently proposed by the U.S. Department of Energy.[15] And while contactors were originally developed for use in spent fuel recycling they have application to liquid–liquid extraction processes used in a variety of fields including chemical processing,[16,17] pharmaceutical production,[18] and oil-water separations.[19,20] The purpose of this research is to improve the general understanding of the flow within a centrifugal contactor through the application of computational fluid dynamics (CFD). The overall goal of this effort is to develop and demonstrate a practical and experimentally validated modeling scheme which can be used to guide contactor design, perform operational optimizations, and help facilitate wider use of centrifugal contactors.

Contactor operation

For solvent extraction processes using a mix/settle stagewise extraction type of equipment (as opposed to a continuous column), the key to successful operation is to achieve efficient mixing of two immiscible fluids by creating small droplets with a large total surface area for good extraction followed by quick separation of the two phases. The annular centrifugal contactor is able to combine both the mixing and separation functions within a single compact device. Flows of immiscible liquids enter through tangential ports into the annular or mixing region where the dispersion forms as the fluids are turbulently mixed by shear induced by the spinning rotor. Stationary radial vanes on the housing below the rotor break the rotation of the dispersion and force the liquid into the rotor which then acts as a centrifuge separating the two phases and pumping the liquid upward. The separated phases then flow over their respective weirs and out the exit lines flowing by gravity to successive stages or collection vessels. In this way the contactor acts as a mixer, a centrifuge, and a pump. Contactors can be set up in a sequential bank of multiple units with countercurrent flow requiring no interstage pumps.

Within the mixing region, under normal operating conditions there is an air space above the mixing liquid such that there is free surface flow (flow of a liquid-gas interface) and gas entrainment. This annular liquid height is an important parameter affecting the mixing and overall extraction efficiency of the contactor. Further, it appears that the majority of mixing occurs in the annulus with the result that for a given rotor speed a greater liquid height results in greater mixing. The annular liquid height has been observed to be a function of the input flow rate, rotor speed, housing geometry (e.g. vane geometry, annular gap size), and rotor geometry.[14,21,22] Note that the annular liquid height is typically measured as the average height of liquid (relative to the rotor bottom) at the outer wall. It is important to understand the combination of factors which affect the annular liquid height and the amount of contact between the fluid and the rotor in order to gain insight into how one might optimize operation for a given set of process conditions. As a step towards that end, this article will present the results of computational modeling and experimental measurements of the flow in the contactor mixing zone.

Methods

Experimental apparatus: Modified CINC V-2

The experiments were done using an annular centrifugal contactor manufactured by Costner Industries Nevada Corporation (CINC) which was originally purchased by Argonne National Laboratory with a nonstandard, transparent acrylic contactor housing with tangential inlets as described by Leonard et al.[14] This contactor has a rotor radius r_r of 2.54 cm and a housing radius r_h of 3.17 cm resulting in an annular gap Δr of 0.63 cm and a radius ratio r_r/r_h of 0.8. To make detailed optical measurements possible, this same contactor unit was further modified such that the lower portion of the housing was replaced with a polished quartz cylinder. A small, triangular quartz window was also placed in the bottom vane plate to allow visualization and measurement of the flow beneath the rotor. The modified contactor is shown in Figure 2. The bottom portion of the rotor, the vane plate, and the bottom support plate has been painted with flat black enamel to reduce reflections. While Figure 2 shows the eight-vane plate in place, four-vane plate geometry (inset) is the configuration used for the data presented in this article. Some flow data for the eight-vane geometry and a curved vane[21] configuration were also collected but are not reported here.

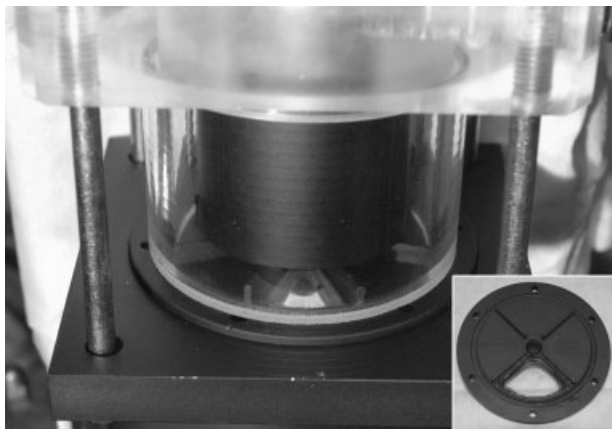

Figure 2. Modified contactor housing with reflective parts painted black.

The four-vane plate which was used for these experiments is shown in the inset.

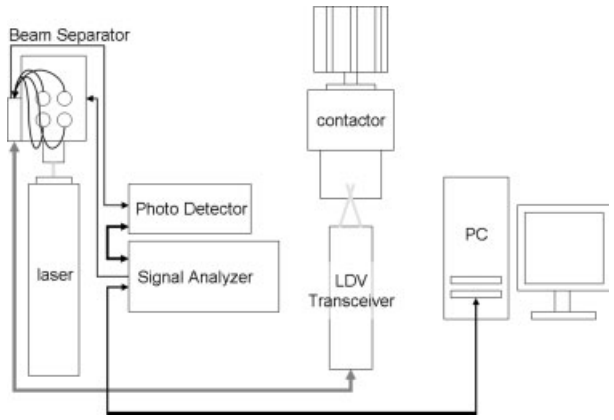

Figure 4. Diagram of the LDV system.

Since the contactor was used only for hydraulic operation with distilled water as the working fluid, the contactor was setup for continuous recirculation as shown in Figure 3. Positive displacement piston pumps manufactured by Fluid Metering Incorporated (FMI) were used for delivering the input flow rate at each of the two tangential inlets. For these experiments the flow rate at each of the inlets was equal, but in practice with actual liquid–liquid extraction this would only be true for an organic-to-aqueous (O/A) flow ratio equal to 1. All of the experiments reported here were performed at a rotor speed of 377 rad/s (3600 RPM) and a total inlet flow rate setting of ~600 ml/min. The actual combined exit flow rate was measured at the heavy phase exit line (by timed flow into a volumetric cylinder) and had an average value of 606 ± 7 ml/min.

Laser doppler velocimetry (LDV)

The LDV apparatus used for these experiments was a 2D LDV system from TSI Incorporated using a two-component fiberoptic transceiver (model TR260) in backscatter mode. The LDV system was controlled and data was acquired using the accompanying FlowSizer 1.1 software. A diagram of the LDV system is shown in Figure 4. The shape and pulse characteristics of the LDV signal from the signal analyzer was also monitored during operation using an oscilloscope.

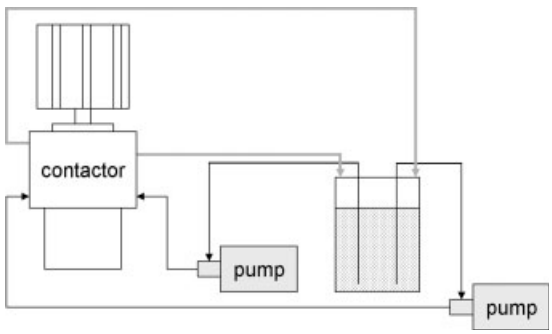

Figure 3. Flow diagram of the continuous recirculation setup that was used during all experimental measurements.

Because of the contactor's annular geometry, only backscatter measurements were possible and, therefore, the transceiver was used rather than an off-axis or forward scatter receiver. The scattering media for the LDV measurements were the entrained air bubbles. While bubbles are generally not ideal flow tracers,[23] due to the violent mixing and free surface flow within the centrifugal contactor they are unavoidable. Much of the discussion regarding the applicability of LDV to bubbly flows focuses on large bubbles (>4 mm) at low volume fraction where one is often interested in distinguishing the bubble velocity from the liquid velocity.[24–26] Such is not the case for the contactor in which the bubbles tend to be small (100–1000 μm) and spherical. Further, regions of the flow can be quite bubbly (see Figure 13) making distinguishing between the bulk liquid velocity relative to the bubbles difficult and less useful. It is assumed that the slip velocity is small and therefore that the measured bubble velocity is representative of the bulk flow. However, to determine if there is a significant effect due to bubble size, the LDV measurements were repeated using water with 25 mg/l sodium dodecylsulphate (SDS). Addition of this surfactant in low concentrations has been shown by others to inhibit bubble coalescence and produce smaller and more uniform air bubbles.[27,28] Initially 50 mg/l SDS was tested, but this resulted in some undesirable foam build-up in the collector ring and storage vessel and consequently the concentration was reduced to 25 mg/l.

The transceiver probe was mounted on a traversing plate that enabled accurate measurement of the relative axial and radial position of the probe. Because of the change in the index of refraction between the air, quartz, and water, the incremental radial motion of the probe is not equal to that of the measuring volume and the measurement positions had to be corrected for these effects. Further, the curvature of the glass also has an effect for the tangential (horizontal) velocity measurements. A 135-mm focal length lens (measuring volume $\approx 34 \times 180\ \mu m^2$) was used on the transceiver probe as this was the shortest focal length lens available and would minimize these beam refraction issues due to the curved window. Because of these curvature effects as well as the changes in refraction indices, a correction to the radial position of the measurement

location was applied to the data based on the ratio of the LDV-measured and known width of the annular gap.

Measurements of tangential and axial velocities were taken for the standard flow conditions (377 rad/s, 600 ml/min) along the radial direction perpendicular to the rotor at four axial positions: at the rotor bottom ($z = 0.00$ cm), near the mid-vane height under the rotor ($z = -0.46$ cm), and at two axial heights above the rotor bottom, $z = 0.61$ cm ($\approx 1 \cdot \Delta r$) and $z = 1.32$ cm ($\approx 2 \cdot \Delta r$). These measurement lines were in the plane which is perpendicular to the inlets and bisects the region between vanes. The total number of measurements at each position varied according to the data rate—where the data rate was high ($\sim$200–1000 Hz), such as near the outside wall, as many as $\sim$16,000 data points were recorded; closer to the rotor, where the data rate was relatively low ($\sim$30–200 Hz), the number of recorded points was always greater than 2000. Where the data acquisition rate was sufficient, the power spectrum was also computed using the FlowSizer software.

High-speed flow imaging

High-speed imaging of the flow in the contactor was performed to provide qualitative observation of the dynamics of the flow in the contactor mixing zone as well as some quantitative observation of the annular liquid height. A Redlake MotionPro (model HS-3-M-4) camera was used for the high-speed imaging. The flow imaging presented here was performed at 1000 Hz for the standard flow conditions, 600 ml/min of water and a rotor speed of 377 rad/s (3600 RPM).

CFD modeling

A preliminary CFD modeling study was performed previously which looked only at single-phase flow in the lower portion of contactor mixing zone.[29] The current simulations presented here provide a more realistic analysis of the flow in the mixing zone by including the free surface flow of water (and air) in the entire mixing zone using the volume of fluid (VOF) interface tracking method with piecewise linear interface construction (PLIC). The VOF technique is widely used for modeling interfacial flows and is capable of capturing complex interface dynamics including interface breakage and reattachment.[30,31] The continuum surface force model[32] was also used to account for surface tension effects on the air-water interface. The CFD modeling was done with Fluent 6.3 in parallel on $\sim$16, 1.3 GHz nodes in a Linux cluster.

The flow in the contactor mixing zone is highly turbulent ($Re = 6 \times 10^4$ at 377 rad/s based on the annular gap), and separate transient simulations using three different turbulence modeling techniques were performed for comparison with the experimental measurements. These were the RNG k-ε model, the large eddy simulation (LES) method, and the detached eddy simulation (DES) method. As detailed comparisons can be found in relevant texts on turbulence modeling,[33] only a brief description of each model will be given here. The RNG k-ε model is a Reynolds Averaged Navier-Stokes (RANS) modeling technique which solves only for the statistical mean flow. This model is particularly suited for swirling flows (a swirl factor of 0.07 was used here) and was determined in some previous simulations of single-phase flow under the rotor[34] to be a good RANS-type model for the flow in the centrifugal contactor. The LES technique fully resolves (solves the full Navier-Stokes equations for the instantaneous velocity field) those turbulent structures which are larger than the grid size and models those which are on the subgrid scale.[33] A turbulent kinetic energy transport subgrid model was used for the LES simulation.[35] The DES technique can be viewed as a hybrid RANS/LES method and was originally developed for application to very high *Re* number aerodynamic flows where fully resolved LES is not feasible. The realizable k-ε RANS model was used for the DES simulations.[35]

All three simulations were done on the same computational mesh. This mesh was generated using Gambit 2.2 from Fluent Inc. Because of the high computational cost of running transient simulations using the VOF model, the mesh density for these simulations was necessarily somewhat coarse. A quadrilateral mesh with spacing of 0.1 cm on the rotor surface and 0.15 cm tetrahedral mesh elsewhere was used to slightly enhance the mesh clustering near the rotor. The resulting mesh had a total number of 286 K computational cells. The time step Δt was allowed to vary such that a Courant number Cr of 0.25 was maintained. The Cr number is given by

$$Cr = \frac{\Delta t}{\Delta x / u} \approx 0.25 \tag{1}$$

where u is the local interface velocity and Δx is the local grid spacing. A Cr number of 0.25 ensures that the time step is sufficiently small that the VOF-tracked fluid interface takes at least four time steps to pass through a computational cell. For operation at 377 rad/s (3600 RPM), the resulting time step was on the order of 30 μs. Calculations were performed using Fluent's noniterative time advancement (NITA) algorithm resulting in a significant speed-up in calculation time per time step. Pressure discretization used the body force weighted method and pressure-velocity coupling was facilitated using the PISO algorithm.[35] The body force weighted scheme was chosen as it is recommended for most free surface flow problems and as it was observed to give better convergence results when using Fluent's NITA solver. The typical solution time was about 100 h/1 s of flow time for all simulations. Because the VOF method requires a transient simulation regardless of the turbulence model and because the same grid was used for all simulations, the increased computational cost of LES as compared with RANS was not significant for the present study.

In regards to the grid density at the walls, the parameter y^+ (Eq. 2) is a dimensionless measure of the near-wall mesh and is a function of the fluid density ρ and viscosity μ, the friction velocity u_τ, and the distance from the wall y.

$$y^+ = \frac{\rho u_\tau y}{\mu} \tag{2}$$

The friction velocity u_τ is determined from the shear stress at the wall τ_w by

$$u_\tau = \left(\frac{\tau_w}{\rho}\right)^{1/2} \tag{3}$$

Note that the y^+ value depends on which fluid (water or air) is in contact with the wall. The average y^+ values in liquid contact regions were $\sim$30 on the housing wall and 40 on the rotor side. Thus standard wall functions (law of the wall), which are applied in Fluent for $y^+ > 30$ were used for all simulations. While the applicability of standard wall models to LES

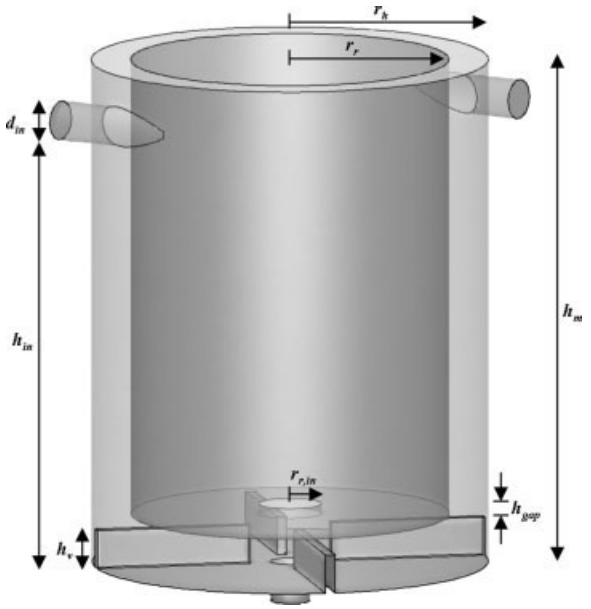

Figure 5. Full mixing zone model geometry with selected dimensions labeled.

Corresponding values are given in Table 1.

has been debated,[36] this study will provide an evaluation of the accuracy of coarse grid LES with wall functions as compared with RANS and DES for the annular centrifugal contactor problem.

Figure 5 shows the geometry for the mixing zone model (Table 1). The top surface is defined as an atmospheric pressure boundary to enable the volume of air (incompressible) in the system to vary and allow the volume of liquid in the mixing zone to reach an equilibrium level depending on the operating conditions (i.e. inlet flow rate and rotor speed) and the mixing zone outlet pressure. The mixing zone outlet pressure was calculated by assuming that the pressure at the center point of the outlet surface is simply equal to the pressure generated by the rotating air column within the separating zone (see Figure 1). The pressure difference at any two points (denoted by subscripts 1 and 2) in the rotating air column within the rotor can be calculated according to the Bernoulli equation for rotating flow

$$P_1 - P_2 = \frac{\rho\Omega^2}{2}(r_1^2 - r_2^2) - \rho g(h_1 - h_2) \tag{4}$$

in which ρ is the mass density of air, Ω is the rotational speed of the rotor, and g is the acceleration due to gravity. As noted on Figure 1, if we choose point 1 to be the less-dense phase rotor outlet (which is assumed to be always open to the atmosphere for single liquid operation below the zero-point flow rate[14]), it is possible to calculate the pressure at the center point on the rotor inlet (point 2). For a rotation rate of 377 rad/s (3600 RPM) the relative pressure at the rotor inlet is found to be slightly negative (>–100 Pa). For these models, the outlet pressure was set equal to –53.6 Pa. Actual measurements of the pressure at the rotor inlet have also been performed which verify that this method gives a reasonably accurate value for the pressure at this boundary.

Table 1. Selected Geometric Parameters of Contactor Mixing Zone Model as Shown in Figure 5

Parameter	Symbol	Value
Rotor Radius	r_r	2.54 cm
Housing Radius	r_h	3.17 cm
Radius Ratio	r_r/r_h	0.801 cm
Rotor Inlet Radius	$r_{r,in}$	0.505 cm
Vane Height	h_v	0.617 cm
Vane-to-Rotor Gap	h_{gap}	0.159 cm
Mixing Zone Height	h_m	8.13 cm
Inlet Bottom Height	h_{in}	7.00 cm
Inlet Diameter	d_{in}	0.63 cm

The simulations were initiated from rest with a stationary water level ~1.5 cm above the rotor bottom and were allowed to run for several seconds of flow time until the liquid volume reached a steady-state level. Time averaging over 0.5 s of flow time was performed for all three turbulence methods. All simulations were done for the same conditions as the experimental measurements, that is, a total mass flow rate of 0.01 kg/s (0.005 kg/s at each inlet ≈ 600 ml/min) and a rotor speed of 377 rad/s.

Results and Discussion

Mean flow field from CFD

The time-averaged flow field obtained from the LES simulations will be described first as it helps lend a visual picture to the quantitative data that will be presented in the next section. Figure 6 shows the time-averaged velocity vectors within a vertical cross-sectional plane—that is, only the radial and axial mean velocity components are included. This highlights the presence of a stable Taylor-Couette cell just above the rotor bottom in which the fluid is moving upward at the rotor and downward at the housing wall. This is consistent with the flow patterns observed in previous single-phase contactor simulations.[29] Above this height at the upper edge of the Taylor-Couette cell where the flow is directed radially outward, the free surface appears to dominate the flow and prevent the formation of any other stable Taylor-Couette vortices in the liquid phase.

Figure 7 shows that below the rotor there are large swirling vortices within each section between vanes in which each vortex is swirling in the direction of rotor rotation (counter-clockwise). Some slight asymmetry is apparent between the regions directly adjacent to the inlets and the other two regions. For the two opposing sections nearest the inlets, the center of each vortex appears slightly shifted towards the forward rotational direction and the vortex is somewhat less compact and circular as compared to the two regions not adjacent to the inlets. The velocity magnitude at the outside wall is also slightly higher for the regions adjacent to the inlets. This results in an eye-shaped crossing flow pattern at the axis of the rotor with flow exiting each vortex in a direction parallel to the forward vane and joining the flow within the adjacent region.

Fluid-rotor contact and annular liquid height (ALH)

Figure 8a shows a snapshot of the instantaneous water volume fraction ϕ (fraction of the given cell that is water) on the rotor side and a vertical cross-section. The air-water interface is also shown ($\phi = 0.5$, green) providing a visualization of the free surface flow in the mixing zone. It is evident that the fluid rotor contact (areas on the rotor side that are red) is not contin-

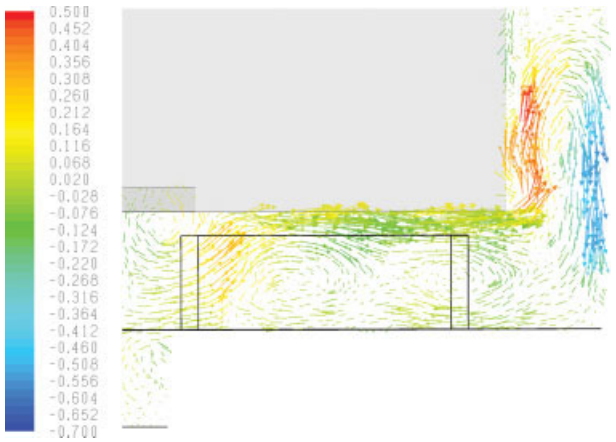

Figure 6. In-plane time-averaged velocity vectors on a vertical cross-sectional plane.

Vectors are colored by mean axial velocity. Only the flow in the lower portion of the model at one side of the rotor is shown.

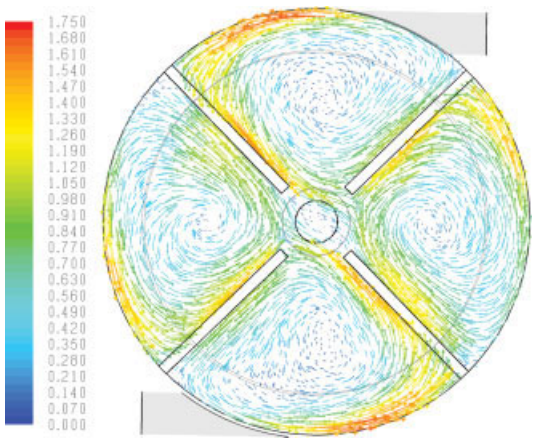

Figure 7. Time-averaged velocity vectors within a horizontal plane under the rotor at the mid-vane height.

Vectors are colored by mean velocity magnitude. Note that the tangential flow inlets are not in the same plane as the vectors (see Figure 5), but are shown to give their position relative to the vanes.

uous. This is also clear from Figure 8b which shows the time-averaged water volume fractions. There is continuous contact between the liquid and rotor for only a height of about $1{\cdot}\Delta r$ above the rotor bottom. Beyond this point contact is intermittent in both space and time although there appear to be some circumferential bands where contact can be as high as 25%.

It was also observed that the liquid height in the annulus varies in time; in fact, it was found that the ALH actually oscillates at near constant frequency and magnitude. The ALH of Figure8a is at an intermediate value for a time where the ALH is increasing from the minimum. This oscillating flow behavior will be discussed in a later section as the frequency and magnitude of oscillation provide valuable points of quantitative comparison between experiment and simulation.

LDV/CFD comparison

This section will present a comparison of the mean and root-mean-squared (RMS) tangential and axial velocity profiles as measured by LDV with those calculated from the CFD simulations using the three different turbulence modeling schemes.

Mean Velocity. The mean tangential and axial velocity components are plotted in Figures 9 where a–d are plots of the mean tangential velocity at the four different axial positions

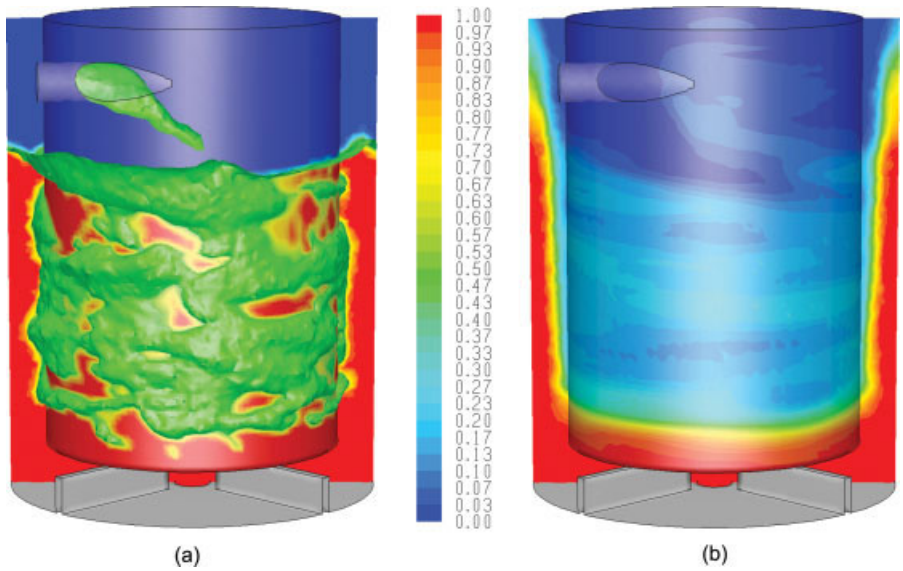

Figure 8. Instantaneous (a) and time-averaged (b) contour plots of water volume fraction ϕ for the four-vane mixing zone geometry.

In (a) the air-water interface is also shown ($\phi = 0.5$, green).

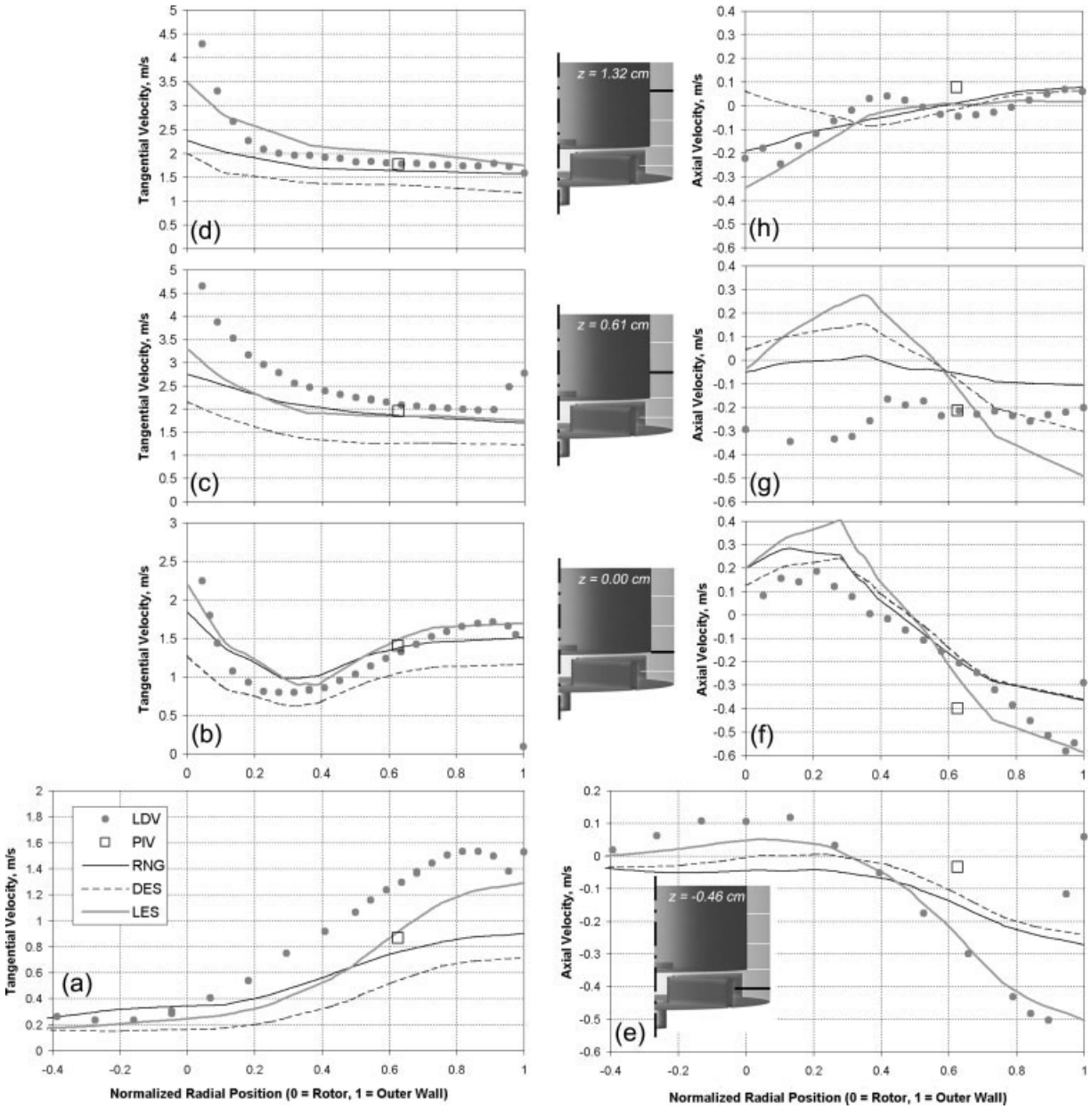

Figure 9. Data plots of the LDV measurements at the four different axial positions as compared to the CFD model predictions for the mean tangential velocities (a)–(d) and the mean axial velocities (e)–(h).

Individual data points from separate particle image velocimetry (PIV) measurements on a vertical plane (perpendicular to the LDV measurement lines) are shown for comparison. The radial position is relative to the rotor side and has been normalized by the gap width Δr.

(with their relative position shown in the insets) and e–h are the corresponding mean axial velocity plots. The time-averaged results from the CFD simulations are also plotted. As one indicator of the relative consistency of the experimental measurements, intersecting points from an initial data set of separate particle image velocimetry (PIV) measurements on a vertical plane (perpendicular to the LDV measurement lines) are also shown. As expected, the tangential velocities are an order of magnitude larger than the axial velocities except for in the vane region. The formation of a stable Taylor-Couette cell (as seen previously in Figure 6) can be seen in Figure 9f in which the flow is upward near the rotor and downward near the housing wall. The CFD models seem to slightly overpredict the height of this rotational cell, however, in that the predicted flow (at least for the LES and DES models) still has a positive axial component near the rotor for the $z = 0.61$ cm position (Figure 9g) whereas the data show a slightly negative axial velocity near the rotor evidencing the start of what would be an upper Taylor-Couette vortex which rotates opposite this lower one.

Aside from the $z = 0.61$ cm height, all of the computational models capture to some degree the main flow characteristics for both velocity components at axial heights above the rotor bottom. However, the LES calculations appear to capture the measured values with greater accuracy. This is particularly evi-

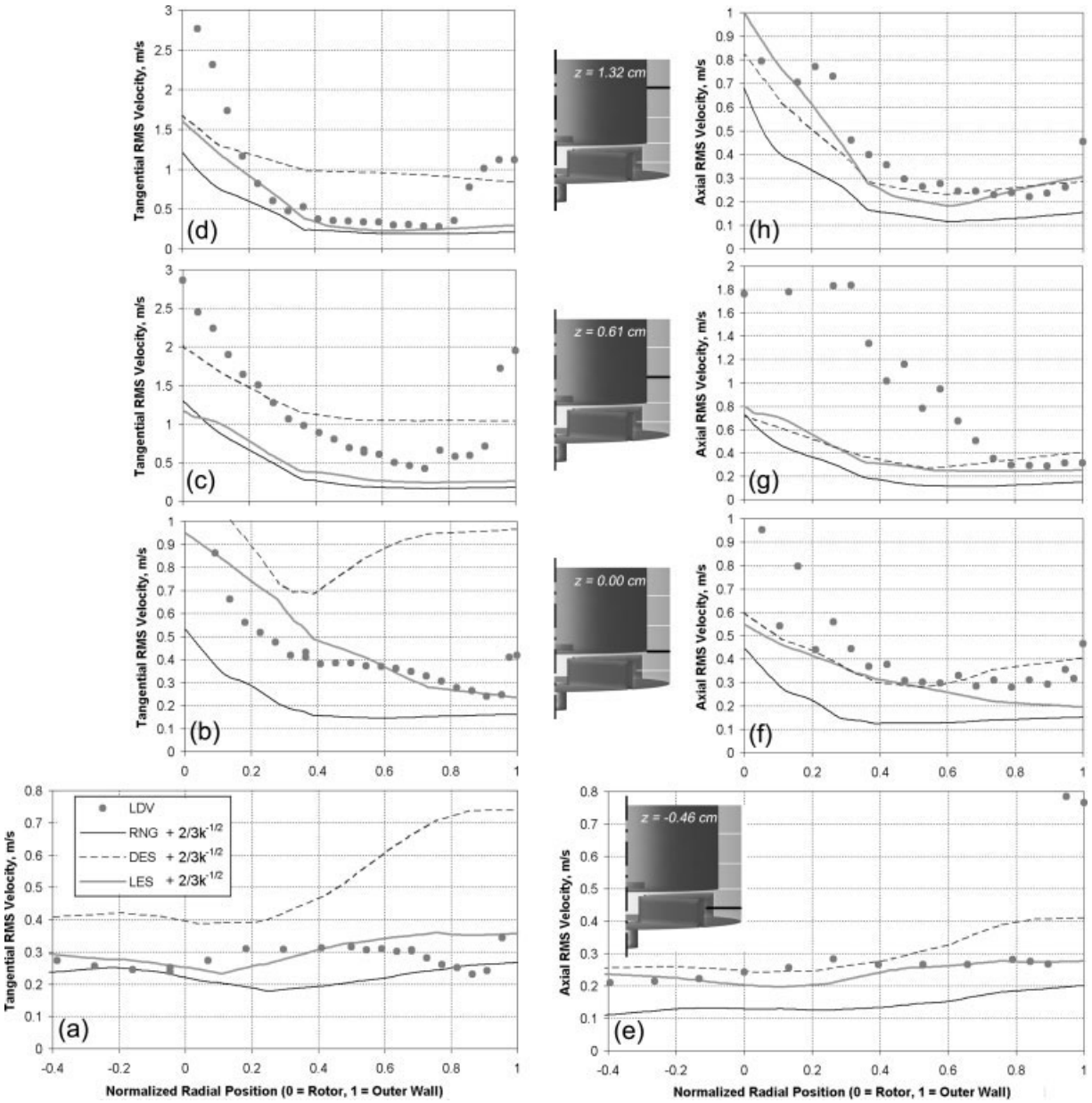

Figure 10. Data plots of the LDV measurements at the four different axial positions as compared to the CFD model predictions for the RMS tangential velocities (a)–(d) and the RMS axial velocities (e)–(h).

dent for the mid-vane height ($z = -0.46$ cm) measurements. The LES model is able to capture the magnitude of the downward flow near the outer wall (Figure 9e) as well as predict a maximum tangential velocity at the same point which is much closer to the measured value than either the RNG or the DES models.

RMS Velocity. The superiority of the LES method is further evident from the corresponding plots of the RMS tangential (Figures 10a–d) and axial (Figures 10e–h) velocity data and simulation results. Note that for both experiment and simulation, the RMS quantities include both the bulk variations in flow velocities caused by the free surface motion as well as the turbulence induced fluctuating component of velocity. Again, none of the models gave very good predictions for the RMS velocity profile at the $z = 0.61$ cm height due to the overprediction of the height of region of continuous liquid-rotor contact and the resulting Taylor-Couette cell. At the other axial heights, the agreement between the LES prediction and measured values is significantly better than the other two turbulence modeling schemes. Interestingly, the DES model tends to severely overpredict the tangential RMS velocity component while at the same time giving results similar to LES for the axial RMS velocity. In virtually all cases, the RANS model underpredicts the actual RMS velocities.

The deviation of the LES model from the experimental values near the rotor is not surprising due to the coarse nature of the computational grid (as compared with traditional LES) and the use of wall functions. However, in order to get an accurate estimation of the mixing behavior in the contactor it will be

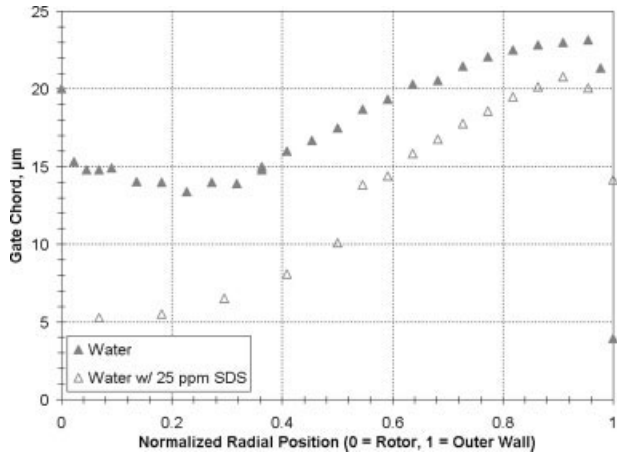

Figure 11. Plot of mean gate chord for the LDV measurements at the rotor bottom height ($z = 0.0$ cm) comparing the LDV measurements with only water with those repeated using 25 mg/l SDS.

necessary to get accurate turbulence predictions near the rotor. It is well known that the mixing behavior of liquid–liquid dispersions is characterized by the maximum rate of turbulent energy dissipation ε_{max}.[37–39] Unfortunately, it was not possible to experimentally measure the dissipation rate near the rotor where the area of maximum dissipations occurs due to the relatively low LDV data rate in this region. However, to provide approximate values for comparison with other liquid–liquid mixing systems the dissipation rates predicted by LES simulation are given here. The LES simulation predicts a maximum subgrid dissipation rate (scaled by liquid phase volume fraction to get liquid phase contribution only) of 900 W/kg on the rotor side with an area-weighted average value of 90 W/kg over the surface of the rotor. The value averaged over the entire mixing zone volume is 12 W/kg. Note that these are instantaneous values taken at the same flow time as Figure 8a.

LDV Measurements with SDS. The LDV measurements presented in the previous section were taken using entrained air bubbles as the scattering media. To explore the effect of bubble size on the consistency of the measurements, some repeat LDV measurements were made using water with 25 mg/l SDS. As a measure of the change in bubble size, Figure 11 gives a comparison of the average "gate chord" measured at the rotor bottom height ($z = 0.0$ cm) for the LDV with pure water and that with the added surfactant. The "gate chord" has been defined as the product of the average fluid velocity [m/s] and the average Doppler signal time (or gate time) [μs] at a given point yielding a quantity of length with units of μm. The change in fluid particle size is clearly evident between the two measurements and shows a decrease of nearly a factor of three close to the rotor. Thus, it appears that the addition of the surfactant causes a measurable decrease in the characteristic length of the air bubbles passing through the LDV measuring volume.

Despite this substantial change in the measured length scale, the measured velocities were not altered significantly. Figure 12 shows the measured mean tangential velocities with both pure water and water with the surfactant as measured at the rotor bottom height. Only a slight change in the magnitude of the measured mean tangential velocity profile is evident. This gives an indication that the LDV measurements in this study may not be strongly dependent on the air bubble size.

Annular liquid height (ALH) oscillations

It was observed both experimentally and through the CFD simulations that the liquid height in the annular mixing zone oscillates at steady frequency and magnitude. Experimentally, this was seen through the use of high-speed video imaging as well as with the LDV measurements. Figure 13 shows two snapshots separated by 0.11 s which show a minimum (a) and successive maximum (b) in ALH. The liquid height at the minimum position is easily distinguishable and appears relatively flat in the circumferential direction. The maximum is difficult to identify from the image as it extends beyond the optical quartz section. From physical observation the average magnitude of the oscillation was observed to be 1.8 ± 0.4 cm. It is also apparent in Figure 13a that there may be a second turbulent Taylor-Couette vortex that forms above the lower one during the time when the liquid is at its minimum height; however, this upper vortex breaks down as the fluid loses contact with the rotor (Figure 13b). The CFD model predicts similar behavior as evidenced by a band of high time-averaged fluid rotor contact above the region of continuous contact (see Figure 8b).

It was possible to determine the frequency of the oscillation as observed by a spike in the power spectrum plots generated by taking a fast Fourier transform (FFT) of the time auto-correlation of the LDV data for measuring points near the outer wall where the data rate was sufficiently high. A representative power spectrum plot is shown in Figure 14 in which the frequency spike from the free surface oscillation is denoted and shows up at 4.85 Hz. Averaging over 24 separate frequency observations, it was determined that the mean frequency of the

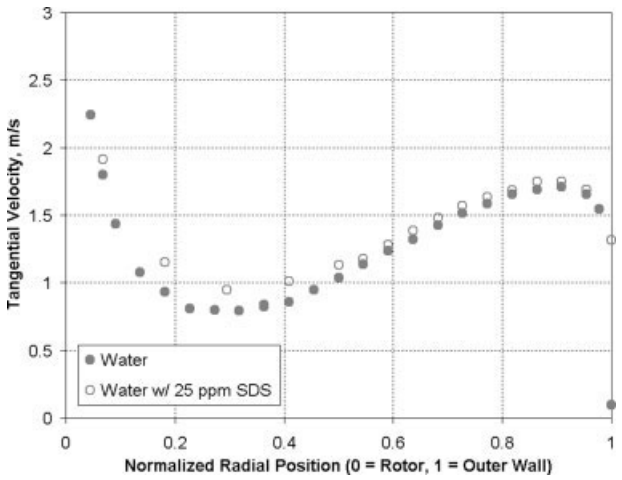

Figure 12. Plot of the mean tangential velocity LDV measurements along the rotor bottom comparing the LDV measurements with only water (same as Figure 9b) with those repeated using 25 mg/l SDS.

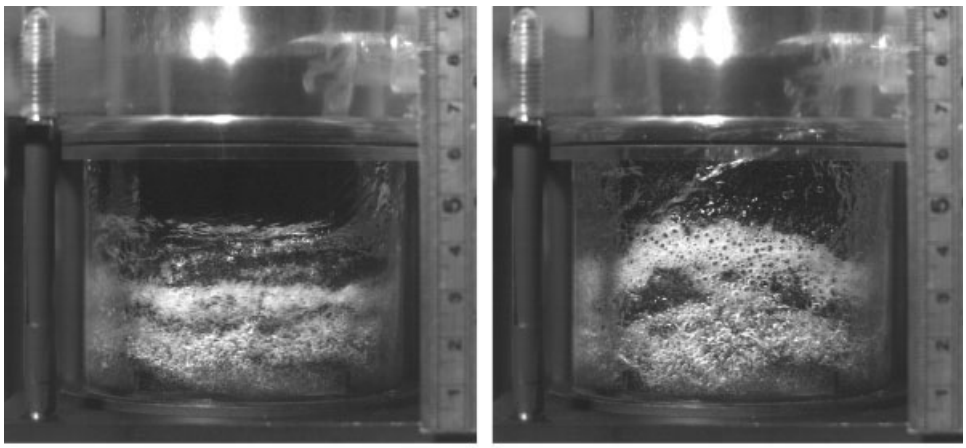

Figure 13. Snapshots of flow in the mixing zone showing a minimum [(a), $t = t_0$] and maximum [(b), $t = t_0 + 0.11$ s] of the liquid height oscillations.

For reference, the rotor bottom is at ~1.3 cm on the ruler. The exposure time was 500 μs.

liquid surface oscillation for the given conditions was 4.75 ± 0.16 Hz.

Similarly, the magnitude and frequency of the ALH oscillation can be predicted by the CFD simulations. The predicted annular liquid height and rotor-side liquid contact area over an arbitrary 1-s period of flow time from an LES simulation of the contactor is given in Figure 15. The ALH in Figure 15 was determined by integrating the area of liquid contact on the housing wall, dividing by the circumference $2\pi r_h$, and subtracting the height of the rotor bottom (0.776 cm); thus it is the circumferentially averaged liquid height above the rotor bottom. The steady oscillation of the liquid height is quite apparent. It can also be seen that the liquid height minima correspond to maximum values in the rotor contact area. In fact, the maximum contact area occurs at the instant just after the liquid height reaches its minimum. This predicted behavior was also verified by the high speed videos in which the fluid contacting the rotor is spun off the rotor and can be seen impinging on the outer wall just after the liquid height falls to the minimum value. For reference, the integrated fluid rotor contact area for the image in Figure 8a is 26.5 cm^2.

From the LES simulations, the average magnitude of the oscillations for an 8-cycle period was found to be 2.19 ± 0.23 cm which is within the range of the experimental value. As for the frequency, taking an average of the trough-to-trough time increment over the same 8 cycles we find an average predicted oscillation frequency of 4.07 ± 0.18 Hz which is somewhat lower than the measured value. This error may simply be a result of the limited grid resolution and future work using more refined meshing will explore this as increased computational resources have currently become available.

A summary comparison of experimental and simulation values for the annular fluid height oscillation are shown in Table 2. While this dynamic behavior may not be surprising—the fluid contacts the rotor, is spun off, and falls back down—it is important to note that it is only observed for the four-vane housing configuration. For the eight-vane housing at the same

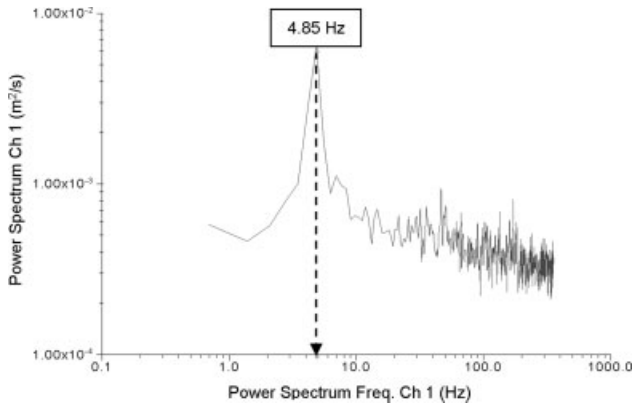

Figure 14. Plot of the power spectrum from a tangential velocity LDV measurement showing the frequency spike indicative of the free surface oscillation.

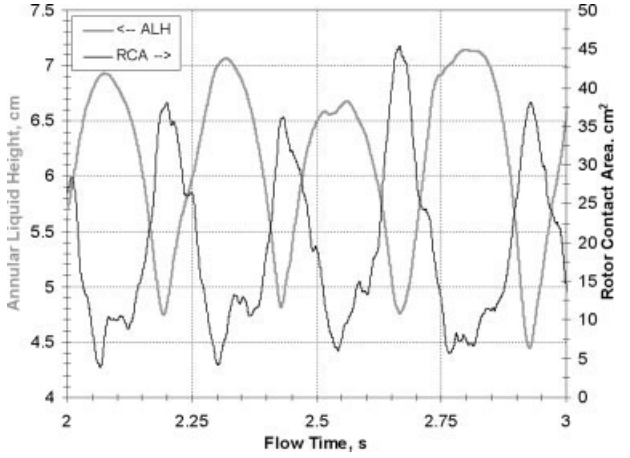

Figure 15. Plot of annular liquid height (left axis, grey) and rotor-side contactor area (right axis, black) for 1 s of flow time showing the CFD (LES) predicted oscillation in ALH.

Table 2. Comparison of Predicted and Measured Values for the Frequency and Magnitude of Liquid Height Oscillation

	Exp	CFD (LES)
Frequency (Hz)	4.75 ± 0.16	4.07 ± 0.18
Magnitude (cm)	1.8 ± 0.4	2.19 ± 0.23

flow conditions, the liquid height is significantly lower (<50%) and does not exhibit the oscillations seen here. The curved-vane geometry also does not produce these liquid height oscillations though the liquid height is somewhat higher than for the eight-vane contactor.[14] It is anticipated that a comparison of the flow for the different vane geometries will be explored in greater detail as part of future studies.

Conclusions

This study has presented a comparison of experimental measurements and computational modeling of the free surface flow in the mixing zone of an annular centrifugal contactor. It was found that CFD modeling using the LES turbulence simulation method even for a relatively coarse computational grid was able to qualitatively and quantitatively predict the actual dynamics of the flow in the contactor mixing zone. Comparison with LDV data showed that the mean and RMS velocities were captured with much better accuracy by LES modeling than for either RANS or DES on the same mesh. Thus, for transient modeling of the flow in the contactor using the VOF interface tracking method, it appears that greater accuracy can be obtained from LES without a significant increase in computational cost. As one purpose of the overall research study is to develop a detailed modeling scheme for use in exploring design and operational optimizations, the trade-off between computational cost and predictive accuracy is critical. More importantly, this study has shown that the velocity predictions and free surface dynamics from CFD modeling of the centrifugal contactor are experimentally verifiable. Thus, these CFD tools can be used with greater confidence to explore and explain the flow in the centrifugal contactor and provide insights into how operation might be improved. Other issues that might be explored through such numerical experiments include those relating to unit scaling as well as the flow and disposition of particulates in the contactor unit. Full computational exploration of these issues, which may not be feasible experimentally, will provide a broader understanding of the fluid dynamics of the annular centrifugal contactor which can aid in the success of used nuclear fuel recycling facilities that will depend on these contactors. Improved understanding of the centrifugal contactor through application of CFD modeling can also help facilitate wider use of this unique piece of process equipment for liquid–liquid extraction in a variety of other fields.

Acknowledgments

The authors would like to acknowledge Argonne National Laboratory for technical support of this research effort. In particular, Kent Wardle would like to thank Candido Pereira and Ralph Leonard of the Chemical Engineering Division for many helpful conversations. This research was performed under appointment to the U.S. Department of Energy Nuclear Engineering and Health Physics Fellowship Program sponsored by the U.S. Department of Energy's Office of Nuclear Energy, Science, and Technology.

Literature Cited

1. Davis M, Jennings A. Equipment for processing by solvent extraction. In: Flagg J, editor. *Chemical Processing of Reactor Fuels*. New York: Academic Press, 1961:271–303.
2. Godfrey J, Slater M, editors. *Liquid–Liquid Extraction Equipment*. West Sussex, UK: Wiley, 1994.
3. Perry R, Green D, editors. *Perry's Chemical Engineers' Handbook*, 7th ed. New York: McGraw-Hill, 1997.
4. Drain F, Vinoche R, Duhamet J. 40 years of experience with liquid–liquid extraction equipment in the nuclear industry. In *Waste Management Symposium, WM'03, February 23–27, 2003, Tuscon, AZ.*
5. Leonard R. Annular centrifgual contactors for solvent extraction. *Sep Sci Technol*. 1980;15:925–943.
6. Leonard R. Recent advances in centrifugal contactor design. *Sep Sci Technol*. 1988;23:1473–1487.
7. Takeda H, Kawata T, Ueda Y, Shimizu R, Nemoto S, Hayashi S. Development of a centrifugal contactor. In: Sekine T, editor. *Solvent Extraction 1990, Proceedings of the International Solvent Extraction Conference*, Kyoto, Japan, July 18–21, 1990, Volume A. Elsevier, 567–572.
8. Law JD, Herbst RS, Peterman DR, Tillotson RD, Todd TA. Development of a cobalt dicarbollide/polyethylene glycol solvent extraction process for separation of cesium and strontium to support advanced aqueous reprocessing. *Nucl Technol*. 2004;147:284–290.
9. Bonnessen PV, Delmau LH, Moyer BA, Leonard RA. A robust alkaline-side CSEX solvent suitable for removing cesium from Savannah River tank waste. *Solvent Extr Ion Exch*. 2000;18:1079–1107.
10. Bernstein G, Grosvenor D, Lenc J, Levitz N. A high-capacity annular centrifugal contactor. *Nucl Technol*. 1973;20:200–202.
11. Duan W, Song C, Wu Q, Zhou X, Zhou J. Development and performance of a new annular centrifugal contactor for semi-industrial scale. *Sep Sci Technol*. 2005;40:1871–1883.
12. Breschet C, Delafontaine G. Operating experience of centrifugal contactors used in a third plutonium purification cycle at the Marcoule reprocessing plant. In: Sekine T, editor. *Solvent Extraction 1990, Proceedings of the International Solvent Extraction Conference*, Kyoto, Japan, July 18–21, 1990. Volume A. 609–614.
13. Candelieri T, Gerardi A, Petrigliano G, Siepe V. New design centrifugal contactor remotely controlled for solvent extraction operations for feed clarification. In *International Conference on Nuclear Fuel Reprocessing and Waste Management, RECOD 87*. Paris, France, Aug. 23–27, 1987, 1143–1153.
14. Leonard R, Raglabuto M, Aase S, Arafat H, Falkenberg J. Hydraulic performance of a 5-cm contactor for caustic-side solvent extraction. Technical Report ANL-02/18, Argonne National Laboratory, Argonne, IL, 2002.
15. The Global Nuclear Energy Partnership: Greater energy security in a cleaner safer world. Available online at www.gnep.energy.gov, 2006.
16. Duan W, Zhou X, Zhou J. Extraction of caffeine with annular centrifugal contactors. *Solvent Extr Ion Exch*. 2006;24:251–259.
17. Zhou J, Duan W, Zhou X, Zhang C. Application of annular centrifugal contactors in the extraction flowsheet for producing high purity yttrium. *Hydrometallurgy*. 2007;85:154–162.
18. Meikrantz D, Macaluso L, Flim W, Heald C, Mendoza G, Meikrantz S. A new annular centrifugal contactor for pharmaceutical processes. *Chem Eng Commun*. 2002;189:1629–1639.
19. Meikrantz D. Method for separating disparate components in a fluid stream. US Patent 4,959,158, 1990.
20. Meikrantz D, Macaluso L. Centrifugal separator. US Patent 5,591,340, 1997.
21. Birdwell JF, Anderson KK. Evaluation of 5-cm centrifugal contactor hydraulic and mass transfer performance for caustic-side solvent extraction of cesium. Technical Report ORNL/TM-2001/137, Oak Ridge National Laboratory, Oak Ridge, TN, 2001.
22. Law J, Tillotson R, Todd T. Evaluation of the hydraulic performance and mass transfer efficiency of the CSSX process with the optimized solvent in a single stage of 5.5-cm diameter centrifugal contactor. Technical Report INEEL/EXT-02-01106, Idaho National Engineering and Environmental Laboratory, Idaho Falls, ID, 2002.
23. Mei R. Velocity fidelity of flow tracer particles. *Exp Fluids*. 1996; 22:1–13.
24. Groen J, Mudde R, Van den Akker H. On the application of LDA to bubbly flow in the wobbling regime. *Exp Fluids*. 1999;27:435–449.

25. Vasallo P, Trabold T, Moore W, Kirouac G. Measurement of velocities in gas–liquid two-phase flow using laser Doppler velocimetry. *Exp Fluids*. 1993;15:227–230.
26. Sheng Y, Irons G. A combined laser Doppler anemometry and electrical probe diagnostic for bubbly two-phase flow. *Int J Multiphase Flow*. 1991;17:585–598.
27. Dai D, Wu Y, Liu Q. Application of emulsifying air bubbles as tracers in PIV. *J Sichuan Univ*. 2000;32:1–3.
28. Wilkins R, Thomas D, Glassmeyer S. Surfactant use for slug flow pattern suppression and new flow pattern types in a horizontal pipe. *J Fluids Eng*. 2006;128:164–169.
29. Wardle KE, Allen TR, Swaney R. CFD study of the flow in an annular centrifugal contactor. *Sep Sci Technol*. 2006;41:2225–2244.
30. Kothe DB, Rider WJ. Comments on modeling interfacial flows with volume-of-fluid methods. Technical Report LA-UR-94-3384, Los Alamos National Laboratory, Los Alamos, NM, 1995.
31. Tang H, Wrobel L. Modeling the interfacial flow of two immiscible liquids in mixing processes. *Int J Eng Sci*. 2005;43:1234–1256.
32. Brackbill J, Kothe D, Zemach C. A continuum method for modeling surface tension. *J Comput Phys*. 1992;100:335–354.
33. Pope S. *Turbulent Flows*. New York: Cambridge University Press, 2000.
34. Wardle KE, Allen TR, Swaney R. CFD study of turbulence in an annular centrifugal contactor. *Trans Am Nucl Soc*. 2006;94:799–800.
35. Fluent Inc. *Fluent 6.2 User's Guide*, Fluent Inc. 2005.
36. Cabot W, Moin P. Approximate wall boundary conditions in the large-eddy simulation of high Reynolds number flows. *Flow Turbul Combust*. 1999;63:269–291.
37. Hinze J. Fundementals of the hydrodynamic mechanism of splitting dispersion processes. *AIChE J*. 1955;1:289.
38. Davies J. Drop size of emulsions related to turbulent energy dissipation rates. *Chem Eng Sci*. 1985;40:839–842.
39. Zhou G, Kresta SM. Correlation of mean drop size and minimum drop size with the turbulence energy dissipation and the flow in an agitated tank. *Chem Eng Sci*. 1998;53:2063–2079.

Manuscript received Aug. 3, 2007, and revision received Oct. 11, 2007.